Published in final edited form as:
Int J Cancer. 2007 November 15; 121(10): 2153–2161. doi:10.1002/ijc.22900.

Modulating metastasis by a lymphangiogenic switch in prostate cancer

Ebba Brakenhielm[1], **Jeremy B. Burton**[2], **Mai Johnson**[2], **Nelson Chavarria**[1], **Kouki Morizono**[3], **Irvin Chen**[3], **Kari Alitalo**[4], and **Lily Wu**[1,2,5,*]

[1]Department of Urology, David Geffen School of Medicine at UCLA, Los Angeles, CA [2]Department of Molecular & Medical Pharmacology, David Geffen School of Medicine at UCLA, Los Angeles, CA [3]Department of Microbiology, Immunology and Molecular Genetics, David Geffen School of Medicine at UCLA, Los Angeles, CA [4]Molecular/Cancer Biology Laboratory and Ludwig Institute for Cancer Research, Helsinki University Central Hospital, Helsinki, Finland [5]Crump Institute of Molecular Imaging, David Geffen School of Medicine at UCLA, Los Angeles, CA

Abstract

Prostate cancer dissemination is difficult to detect in the clinic, and few treatment options exist for patients with advanced-stage disease. Our aim was to investigate the role of tumor lymphangiogenesis during metastasis. Further, we implemented a noninvasive molecular imaging technique to facilitate the assessment of the metastatic process. The metastatic potentials of several human prostate cancer xenograft models, LAPC-4, LAPC-9, PC3 and CWR22Rv-1 were compared. The cells were labeled with luciferase, a bioluminescence imaging reporter gene, to enable optical imaging. After tumor implantation the animals were examined weekly during several months for the appearance of metastases. Metastatic lesions were confirmed by immunohistochemistry. Additionally, the angiogenic and lymphangiogenic profiles of the tumors were characterized. To confirm the role of lymphangiogenesis in mediating metastasis, the low-metastatic LAPC-9 tumor cells were engineered to overexpress VEGF-C, and the development of metastases was evaluated. Our results show CWR22Rv-1 and PC3 tumor cell lines to be more metastatic than LAPC-4, which in turn disseminates more readily than LAPC-9. The difference in metastatic potential correlated with the endogenous production levels of lymphangiogenic growth factor VEGF-C and the presence of tumor lymphatics. In agreement, induced overexpression of VEGF-C in LAPC-9 enhanced tumor lymphangiogenesis leading to the development of metastatic lesions. Taken together, our studies, based on a molecular imaging approach for semiquantitative detection of micrometastases, point to an important role of tumor lymphatics in the metastatic process of human prostate cancer. In particular, VEGF-C seems to play a key role in prostate cancer metastasis.

Keywords

lymphatics; vascular endothelial growth factor; lung; luciferase; lymph node

Prostate cancer affects 1 out of every 6th man in the U.S.[1] Already at first diagnosis about 20–30% of patients present with advanced stage disease, for which the therapeutic approaches include radical prostate surgery and hormone ablation. This group of patients is at increased

*__Correspondence to:__ Department of Urology, MRL 2210, Box 951738, University of California, Los Angeles, CA 90095-1738, USA. Fax: 1310-206-5343. lwu@mednet.ucla.edu.
The first two authors contributed equally to this work.

risk of tumor progression after therapy, through the development of androgen-independent disease and metastasis, for which there currently is no effective treatment. During 2006 prostate cancer was estimated to claim around 30,000 lives,[1] making it the second most common cause of cancer mortality in men.

Metastasis is a multistep process where tumor cell dissemination to distal sites occurs through the blood or lymphatic system. Lymph nodes, together with bone and liver, represent the most common sites of metastasis in prostate cancer. For example, pelvic lymph node metastases have been reported in 50–60% of advanced-grade prostate cancer patients,[2–4] and is considered as the strongest predictor of disease recurrence and progression.[5–7] Further, the risk of dying from prostate cancer within 5 years after radical prostatectomy is increased up to 6-fold depending on the degree of lymph node involvement.[8] Thus, the lymphatic vasculature may be the most common path for dissemination in prostate cancer similar to in breast cancer.[9,10] Tumor cells may gain access to the lymphatic circulation either *via* migration towards pre-existing lymph vessels or by stimulation of lymphatic sprouting into the tumor through secretion of lymphangiogenic growth factors.[11,12] In recent years, the complex regulation of lymphangiogenesis has begun to unravel, through the discovery of specific markers for lymphatic endothelial cells and their selective growth factors and receptors.[13] Many clinical studies have found that elevated lymphangiogenic growth factor expression in the tumor, the presence of tumor lymphatics and/or lymph node micrometastases correlate with poor prognosis and distal organ metastasis.[11] The best studied example is breast cancer, where clinical assessment of sentinel lymph node involvement is becoming the standard for diagnosis, prognosis and therapeutic guidance. For prostate cancer, several clinical studies have similarly shown correlations between elevated lymphangiogenic growth factor expression in the tumor and lymph node metastasis and advanced-stage disease.[14–17] Despite these indications, only recently have some experimental data emerged concerning the occurrence of lymphangiogenesis in animal models of prostate cancer,[18,19] thus highlighting the need for further studies to delineate the role of the lymphatic system to guide the development of novel tools for prevention and treatment of prostate cancer metastasis.

In our study we have investigated the impact of tumor lymphangiogenesis on prostate cancer metastasis. We first examined and compared the metastatic potential of 2 recent xenograft models of human prostate cancer, LAPC-4 and LAPC-9.[20,21] These models recapitulate many characteristics of the human disease: (*i*) the tumor cells express *wt* androgen receptor, (*ii*) the tumor growth is relatively slow and androgen-dependent, (*iii*) the tumor cells express prostate specific antigen (PSA). Additionally, we compared the metastatic tendencies and vascular growth factor expression levels of these 2 models to the highly aggressive prostate cancer cell lines CWR22Rv-1 and PC3. Further, to directly query the causative role of tumor lymphangiogenesis in mediating tumor metastasis we evaluated the influence of overexpression of the lymphangiogenic growth factor VEGF-C on metastasis in the weakly metastatic LAPC-9 tumor model. These respective goals were achieved by a noninvasive optical bioluminescence imaging approach that enabled us to monitor the development of distant metastasis in real-time and to locate and quantify micrometastatic lesions in isolated tissues.[22,23] We show here that lymphangiogenesis and VEGF-C expression correlated with lymph node and lung metastasis in the 4 different prostate cancer cell lines examined. Further, we demonstrate that overexpression of VEGF-C resulted in the stimulation of tumor lymphangiogenesis generating a switch from a low-metastatic to a highly-metastatic tumor.

Material and methods

All handling of animals was performed in accordance with the University of California, Los Angeles (UCLA) Animal Research Committee guidelines. Prostate epithelial cell basal medium (PrEBM) and Bulletpack supplements were obtained from Clonetics (San Diego, CA).

Tumor cells

The androgen-dependent human prostate cancer cell lines, LAPC-4 and LAPC-9, derived as previously described,[20,21,24] were kind gifts from Dr. Charles Sawyers (UCLA, Los Angeles, CA). The cells were maintained by *in vivo* passage as subcutaneous xenograft tumors in male severe combined immune-deficient (scid) natural killer cell knock-out ($NK^{-/-}$) mice (Taconic farms; Germantown, NY). During *in vitro* manipulations these cells were seeded in PrEBM supplemented with bovine pituitary extract, insulin, hydrocortisone, GA-1000, retinoic acid, transferrin, T_3, epinephrine and human EGF (Bulletpack, Clonetics). The tumor cells were reimplanted within 3 days of *in vitro* culture. The CWR22Rv-1 and PC3 tumor cell lines (kind gifts from Dr. David Agus, Cedars-Sinai Medical Center, Los Angeles, CA) were maintained *in vitro* in RPMI and DMEM, respectively, containing 10% FBS and 1% Penicillin/Streptomycin.

Lentiviral production and tumor transduction

Before each experiment, fresh LAPC-4 and LAPC-9 tumor tissues were collected to prepare single cell suspensions. Tumor cells were transduced using lentivirus carrying CMV promoter-driven firefly luciferase (FL) or renilla luciferase (RL) reporter genes, as previously described.[25] Briefly, the luciferase genes were sub-cloned from phFL-cmv or phRL-cmv (Promega, Madison, WI) plasmids and inserted downstream of the hCMV promoter in the pCCL-M4 lentiviral vector,[26] resulting in the pCCL-cmv-luciferase-M4 vector used to generate LAPC-4-cmv-FL (hereafter referred to as LAPC-4), LAPC-9-cmv-FL (LAPC-9), LAPC-9-cmv-RL, CWR22Rv-1-cmv-RL (CWR22Rv1) and PC3-cmv-RL (PC3). In a second experiment, LAPC-9 tumors expressing RL were transduced in suspension with lentiviral vector pCCL-VEGFC-IRES-eGFP (LAPC-9/VEGF-C) or empty vector control pCCL-IRES-eGFP (LAPC-9/GFP). Recombinant lentivirus was produced by calcium phosphate cotransfection of 293T cells. Tumor cells were infected using viral supernatant at MOI 1 or 2 during 4 hr of incubation. Robust and constitutive cellular expression of luciferase enzymes were confirmed by an *in vitro* bioluminescence assay (Promega).

In vivo and *ex vivo* optical imaging of primary tumor growth and metastasis

One million lentiviral-transduced tumor cells (LAPC-4, LAPC-9, LAPC-9/GFP, LAPC-9/VEGF-C, CWR22Rv-1 or PC3) expressing FL or RL reporter genes were subcutaneously implanted in the right upper back of immune-deficient male scid/$nk^{-/-}$ mice ($n = 6–10$). Tumor sizes were measured regularly using digital calipers. After administration of luciferase substrates ($_D$-luciferin, 150 mg/kg i.p. for FL; coelenterazine, 1 mg/kg i.v. for RL) the anaesthetized mice were imaged using the bioluminescence optical imager (IVIS 200; Xenogen, Alameda, CA) immediately after tumor implantation and weekly thereafter according to previously described techniques.[22,27] Maximal luciferase signals were semiquantified using Living Image 2.5 (Xenogen) and IGOR (Wavemetrics, Lake Oswego, OR) image analysis softwares. Bioluminescence *in vivo* signal was considered positive if the signal in the region of interest (ROI) exceeded 1×10^5 photons/sec/cm^2/steradian (p/s/cm^2/sr).

The primary tumors were grown to the ethical limit of 15 mm in diameter, at which time the animals either were sacrificed or the tumors surgically removed, as indicated. After operation, the mice were analyzed weekly by optical imaging to monitor the occurrence of metastases. The mice were sacrificed within 100 days postoperation or earlier if either primary tumors regrew or other adversary health signs developed. Upon sacrifice of all animals, the whole body and free-dissected organs were imaged *ex vivo* for bioluminescence after a brief application of luciferase substrate. Data are reported as the average of maximal bioluminescent signals in the ROI and in the unit of p/s/cm^2/sr.

Immunohistochemistry

Tumors, lungs and lymph nodes were processed for histological examination (n = 6–9). Paraffin-embedded sections (5 μm) were stained for a vascular endothelial marker (biotinylated rat anti-mouse CD31 1:100, BD Biosciences, San Jose, CA), lymphatic endothelial markers (rabbit anti-LYVE-1 1:300, RELIATech, Braunschweig, Germany; rabbit anti-Prox1, 1:100, Novus Biologicals, Littleton, CO; and rabbit anti-VEGF receptor (VEGF R)-3, 1:200, Santa Cruz Biotechnology, Santa Cruz, CA), a macrophage marker (rat anti-F4/80, 1:100, AbD Serotech, Raleigh, NC), or a prostate epithelial marker (mouse anti-human pan cytokeratin 1×, Biogenex, San Ramon, CA) as previously described.[28] HRP-conjugated secondary reagents (Vector Laboratories, Burlingame, CA) were detected either using the chromogen diaminobenzidine or fluorescent conjugates (NEN TSA kits, Perkin Elmer, Boston, MA). Confocal microscopic images were taken at 10× or 20× optical magnification using a Carl Zeiss LSM 310 Laser Scanning Confocal microscope.

Images were processed using Photoshop software (Adobe systems, San Jose, CA). For each histological analysis 6–9 animals were included with 5–20 micrographs per animal. Blood or lymphatic vessel profiles (vascular density and vessel lumen sizes) were analyzed in pictures at 10× or 20× optical magnification using a stereological approach as previously described.[29] Briefly, blood vessels were analyzed in sections stained with CD31 and lymphatic vessels were analyzed in sections double labeled for CD31 and LYVE-1 to discriminate between blood and lymphatic vessels. Lymphatic vessels within the tumor and close to the peripheral tumor border were classified as intratumoral vessels, whereas LYVE-1 positive structures outside the tumor border were classified a peritumoral lymphatics.

Real time RT-PCR

Fresh tumor tissue was snap frozen in liquid nitrogen, and stored at −80°C until analysis. The tissue was ground to a fine powder in liquid nitrogen and RNA was extracted using Tri-reagent (Sigma-Aldrich, St Louis, MO) according to the manufacturer's suggested protocol. RNA (1 μg) was reverse transcribed by incubation for 1 cycle at 25°C for 10 min, 48°C for 45 min and 95°C for 5 min. Reaction conditions were as follows: 1× RT-buffer, 5.5 mM $MgCl_2$, 500 μM dNTP, 2.5 μM random hexamer primer, 0.4 U/μl RNase inhibitor and 1.25 U/μl reverse transcriptase enzyme. For each sample, 1 μl cDNA (~ 20 ng) was amplified using SyBr green 2× master mix (Applied Biosystems, Foster City, CA) and 10 μM of the following primers:

Actin:

- forward 5′ TCAAGATCATTGCTCCTCCTGAGC 3′
- reverse 5′ TACTCCTGCTTGCTGATCCACATC 3′

hVEGF-C:

- forward 5′ CGGCTTATGCAAGCAAAGATCTGG 3′
- reverse 5′ GCCTCCTTTCCTTAGCTGACACTT 3′

hVEGF-A:

- forward 5′ AGGAGTACCCTGATGAGATCGAGT 3′
- reverse 5′ CATGGTGATGTTGGACTCCTCAGT 3′

The reaction was run on an Opticon Monitor 2 real time PCR machine (MJ Research/Biorad, Waltham, MA). Samples were amplified using Opticon Monitor 2 real time technology under the following cycling conditions: 39 cycles of 95°C/15 sec, 60°C/30 sec and 72°C/30 sec. Gene expression was determined by standard curve method and normalized to β-actin expression (n = 4 tumors per group).

Statistical analysis

Student's two-tailed *t*-test was used to calculate statistical differences between 2 groups. $p < 0.05$ was considered significant.

Results

Characterization of the LAPC-4 and LAPC-9 *wt* tumors

One million LAPC-4 or LAPC-9 tumor cells overexpressing FL were implanted in the right upper back of immune-deficient mice. The expression level of FL was similar in both tumor cell lines, at $5–7 \times 10^5$ relative light units/s/μg protein as measured *in vitro* prior to implantation. The animals were investigated using bioluminescence imaging immediately after implantation and weekly thereafter. The LAPC-4 tumors established at a slightly slower rate than the LAPC-9 tumors (Fig. 1a). The tumor growth was mirrored by an exponential increase in the emitted *in vivo* luciferase signal (Figs. 1b and 1c). Tumors were surgically removed when they reached the upper ethical limit. The *in vivo* optical signal from the primary tumors at the time of resection was between $1.1–1.4 \times 10^9$ p/s/cm^2/sr, and the sizes of the removed tumors were similar in both groups (data not shown). Detailed immunohistochemical analysis revealed that there were no differences in the degree of vascularity between LAPC-4 and LAPC-9 tumors, as determined by the evaluation of both vessel numbers and vessel sizes (Fig. 1d, data not shown).

In vivo and *ex vivo* optical monitoring of the development of metastases

Because of light scattering properties *in vivo*, low-intensity bioluminescence emitted from micrometastatic lesions may be difficult to detect in the presence of a strong bioluminescence signal produced by primary tumors.[30] Thus, the surgical resection of primary tumors performed in our study not only mimics therapeutic intervention in the clinic but also removes the intense bioluminescence focus thus enabling sensitive monitoring of metastasis development *in vivo*. Immediately after primary tumor removal no signs of secondary lesions were observed. However, within 3 weeks some mice in the LAPC-4 group showed significant optical signals emitted from the ventral side, in a position suggestive of lung metastasis. The further development and growth of these potential metastatic lesions was monitored up to 100 days after the primary tumor removal or until adversary health signs developed (Figs. 2a and 2c). During this time, 7 out of 9 mice in the LAPC-4 group acquired strong luciferase signals in locations distant from the primary tumor implantation site. No such *in vivo* imaging signals were found in the LAPC-9-implanted mice (Figs. 2b and 2c). Tumor regrowth in the surgical site occurred in 5 out of 7 (71%) LAPC-9 mice and in 4 out of 9 (44%) LAPC-4-implanted mice. Thus animals were evaluated at sacrifice to confirm the specific location of metastases by *ex vivo* imaging of dissected organs. In the LAPC-4 group 100% (9 out of 9) of the animals had developed optically detectable metastatic lesions, primarily in lung and regional lymph nodes (Table I, Figs. 2d and 2e), with an average *ex vivo* lung metastatic signal intensity of 3.9×10^7 p/s/cm^2/sr. In contrast, optical signs of metastases could only be found in less than 29% (2 out of 7) of LAPC-9-implanted mice, where positive signals were observed in 1 lung and in 1 brachial lymph node, respectively (Table I, Fig. 2f). Furthermore, these signals were comparably weaker; at less than 12% of the optical intensity observed in LAPC-4-implanted mice.

Immunohistochemical analyses of primary tumors and metastases

To confirm the metastatic lesions identified by optical imaging, the lungs and lymph nodes were retrieved for immunohistochemical analyses. Both LAPC-4 and LAPC-9 tumor cells could be easily distinguished using human cytokeratin as a marker, as seen by the intense cytoplasmic staining in the primary tumors (Fig. 3a). Lymph nodes from the LAPC-4 group

with positive optical signals were found to contain tumor masses involving up to 50% of the nodal area in brachial or cervical lymph nodes (Fig. 3b). Similarly, the tumor cells present in the lung stained strongly for cytokeratin, making identification of metastases straightforward (Fig. 3c). Multiple metastatic lesions were found in lungs from the LAPC-4 group, confirming the results of the optical imaging (Fig. 3d). The 1 LAPC-9 animal with optical signal emitted from the lungs was also verified to carry lung metastases, whereas all other lungs of the LAPC-9 cohort were negative (data not shown).

Evaluation of the angiogenic and lymphangiogenic profiles of the primary tumors

To investigate the presence of tumor lymphatics immunohistochemical analyses were performed on paraffin-embedded primary tumor sections. Samples were double stained to visualize blood and lymph vessels simultaneously. In LAPC-4 tumors, LYVE-1-positive structures were present in the tumor periphery, and thin lymphatic vessels were found penetrating into the tumor, often alongside clusters of blood vessels (Figs. 3e and 3f). The lymphatic nature of these structures was confirmed by staining for murine VEGFR-3 (Fig. 3g). In contrast, LAPC-9 tumors were generally lacking intratumoral lymphatics, except for occasional small lymph vessels close to the tumor border (Figs. 3e and 4d).

To determine if the observed differences in tumor lymphatics were due to differences in vascular growth factor expressions, real time RT-PCR analyses were performed. LAPC-4 tumors showed a slight 1.6-fold increase in vascular endothelial growth factor (VEGF)-A expression levels as compared to LAPC-9 tumors, although it did not reach significance (Fig. 3h). This is in line with our finding that these tumors were equally vascularized. In contrast, the expression of the lymphangiogenic factor VEGF-C was significantly elevated in LAPC-4, at 3.3-fold higher levels as compared to LAPC-9 ($p = 0.01$, Fig. 3h), in agreement with the tumor lymphatics results earlier. The difference in VEGF-C expression levels in LAPC-4 compared to LAPC-9 tumors is modest in this current cohort of animals. Consistently, during the last 2 years, we have observed VEGF-C expression levels in LAPC-4 tumors ranging from 10- to 30-fold higher than in LAPC-9 tumors. This suggests that a downward drift of VEGF-C expression may be occurring in this LAPC-4 model during serial passage in scid mice.

Overexpression of VEGF-C mediates prostate cancer metastasis

To gain further insight into the role of tumor lymphatics in prostate cancer metastasis we used 2 approaches: (*i*) to examine several additional prostate cancer models as to the relation of VEGF-C expression and metastasis and (*ii*) to determine the effects of forced expression of VEGF-C in the low-metastatic LAPC-9 tumor model. The mRNA expression levels of VEGF-C were determined by quantitative RT-PCR in several prostate cancer tumor models, including CWR22Rv-1, PC3, LAPC-4, LAPC-9/GFP and VEGF-C-overexpressing LAPC-9 tumors (Fig. 4a). Among these, the androgen-independent, aggressive PC3 and CWR22Rv-1 tumors showed notably higher VEGF-C expression levels as compared to the androgen-dependent LAPC-4 tumors. This finding is in support of the previously published lymphatic metastatic ability of the PC3 cell line.[31] As expected, overexpression of VEGF-C in the LAPC-9 cell line using a lentiviral approach produced a robust increase in VEGF-C mRNA levels, ~2.5-fold above the level in PC3 tumors. The expression of another pro-lymphangiogenic growth factor in the VEGF family, VEGF-D, was also examined. In contrast to VEGF-C, the level of VEGF-D mRNA was negligible in all 4 prostate tumor models (data not show).

Although VEGF-C is a dominant lymphangiogenic growth factor by activating VEGFR-3,[13] it may also induce angiogenesis by binding to VEGFR-2.[32] Thus, in investigating the effects of overexpression of VEGF-C in LAPC-9 we examined the angiogenic and lymphangiogenic profiles of the tumors in detail. One million tumor cells marked with RL were implanted in the right upper back of immune-deficient mice. The LAPC-9/VEGF-C tumors showed similar *in*

vivo growth rate to the LAPC-9/GFP control tumors as judged by tumor volume measurements (Fig. 4b) and bioluminescence signal evaluation (data not shown). The excised primary tumors were examined by immunohistochemistry to determine their vascular profiles. Intratumoral lymph vessels were much more abundant in LAPC-9/VEGF-C tumors as compared to LAPC-9/GFP control tumors that only contained few peritumoral lymphatics (Fig. 4c–4f). The overexpression of VEGF-C in LAPC-9 resulted in a slight increase in blood vessel density, whereas there was a striking 20-fold increase in intratumoral lymphatic vessel density (Fig. 4c). Indeed, extensive networks of intratumoral lymph vessels, consistently associated with blood vessels, were found in LAPC-9/VEGF-C tumors (Fig. 4e). The anti-murine LYVE-1 staining specifically identified lymphatic vessels as LYVE-1 positive structures were found to be distinct from CD31 positive blood vessels (Figs. 3e and 4e), and expressed VEGFR3 (Fig. 3g) as well as prox1 (Fig. 4e). Further, the LYVE-1 positive cells in the tumors were distinct from tumor-associated macrophages (Fig. 4f).

Next, several different prostate xenograft models were examined for signs of metastasis using bioluminescence imaging at the time of sacrifice. In agreement with the observed elevated expression of VEGF-C, the PC3 and CWR22Rv-1 tumor-bearing animals were found to develop prominent metastases to ipsilateral brachial and axillary lymph nodes, as well as to lung (Fig. 5a). In contrast, the LAPC-9/GFP-implanted control mice showed no signs of metastasis (0 out of 6). However, the induced overexpression of VEGF-C in LAPC-9 tumors was sufficient to potently induce both lymph node and lung metastasis (Fig. 5b). Indeed, 63% (5 out of 8) of the LAPC-9/VEGF-C-implanted mice showed signs of lymph node metastasis, which in 60% of the mice further led to the development of lung metastases (3 out of 5). The bioluminescence intensities of the optical signals were significantly higher in regional lymph nodes and lungs from LAPC-9/VEGF-C-implanted mice as compared to LAPC-9/GFP-implanted control mice (Fig. 5b). These metastatic lesions in lymph nodes (Fig. 5c) and lungs (Fig. 5d) were confirmed by immunohistochemistry. Notably, the sizes of the lesions found by immunohistochemical analysis correlated with the observed bioluminescence signal intensities (Figs. 5c and 5d).

An additional role for VEGF-C in mediating metastasis has been suggested recently, where tumor cell expression of VEGFR-2 or VEGFR-3 may lead to VEGF-C-stimulated tumor cell proliferation and migration in an autocrine fashion,[33,34] resulting in enhanced tumor invasiveness and metastasis. To exclude this possibility the expression levels of VEGFR-3 in LAPC-4 and LAPC-9 tumor cells were examined by real time RT-PCR as well as by immunohistochemistry. We found that both LAPC-4 and LAPC-9 tumor cells completely lacked expression of VEGFR-3 (data not shown), indicating that the VEGF-C mediated enhancement of tumor metastasis was not due to autocrine stimulation in these models.

Discussion

Previous studies from our group have revealed the metastatic nature of LAPC-4 tumors,[22] whereas LAPC-9 tumors rarely metastasize from a subcutaneous implantation site. Hence, in our study we set forth to investigate the metastatic process and to compare the metastatic potential of these 2 models in a more quantifiable manner using molecular imaging. Findings from these recent LAPC models are likely to reflect the behaviors of slower growing, androgen-dependent prostate cancers found in the clinic. Further, we carried on to compare these LAPC models to more aggressive, androgen-independent tumors. Of note, LAPC-4 was originally derived from a regional lymph node metastase in a prostate cancer patient, whereas LAPC-9 originates from a femoral metastase.[20,24] Similarly, the PC3 cancer cell line originates from an aggressive bone metastasis, and has previously been shown in animal models to metastasize to lymph nodes, brain, lung and femurs.[31] In contrast, the CWR22 cell line originates from a nonmetastatic primary prostate cancer lesion, of which CWR22Rv-1 represent an androgen-

independent xenograft subclone with capacity to metastasize mainly to lung, liver and bone in mice.[35,36]

To elucidate the underlying molecular mechanisms of metastasis, the angiogenic and lymphangiogenic profiles of these xenograft models were compared. We found that prostate cancer metastasis correlated with the production level of lymphangiogenic growth factor VEGF-C and with tumor lymphangiogenesis. Among the 4 prostate cancer models analyzed, the 2 most aggressive, androgen-independent lines, PC3 and CWR22Rv-1, expressed the highest levels of VEGF-C and readily disseminated to regional lymph nodes and lung. The elevated VEGF-C expression of the PC3 model has previously been documented in the literature.[18,31,37] In our experience, the CWR22Rv-1 tumors exhibit abundant peritumoral and intratumoral lymphatic vessels (Burton *et al.*, unpublished data). In comparing the 2 slower growing, androgen-dependent LAPC-4 and -9 models, the former was found to express elevated levels of VEGF-C concomitant with the occurrence of intratumoral lymphatics. This moderate stimulation of lymphangiogenesis was sufficient to induce tumor metastasis in all animals bearing LAPC-4 tumors, albeit with a prolonged latency of metastasis as compared to PC3 and CWR22Rv-1 models. In contrast, LAPC-9 tumors, expressing the lowest VEGF-C among the 4 models and lacking intratumoral lymphatics, did not metastasize. In further support of a predominantly lymphatic route of metastasis we found that induced overexpression of VEGF-C in the weakly metastatic LAPC-9 prostate cancer model resulted in stimulation of lymphangiogenesis leading to a highly metastatic tumor phenotype. Specifically, the fact the angiogenic profiles (*i.e.*, the degree of vascularity and the level of expression of VEGF-A between LAPC-4 and LAPC-9 tumors or between LAPC-9/VEGF-C and LAPC-9/GFP control tumors) were comparable indicates that angiogenesis is likely not the key factor accounting for the tumors differential abilities for metastatic spreading in our animal models. In contrast, the main factor seems to be molecular differences related to tumoral lymph vessels.

Our conclusion that tumoral lymphatic vessel content is the major factor accounting for the tumor's metastatic ability is supported by the following findings: (*i*) Metastases were observed in ipsilateral regional lymph nodes in the expected primary lymph drainage pathways, indicative of a lymphatic route of tumor dissemination. (*ii*) VEGF-C, a lymphangiogenic growth factor, was expressed at 3.3-fold higher levels in metastatic LAPC-4 tumors as compared to in low-metastatic LAPC-9 tumors. (*iii*) Peritumoral and especially intratumoral lymphatics were comparatively more abundant in LAPC-4 than in LAPC-9 tumors. (*iv*) Notably enlarged tumoral lymphatic networks were found after overexpression of VEGF-C in LAPC-9 tumors, resulting in a significantly increased density of intratumoral lymphatics as compared to LAPC-9 control tumors. (*v*) Overexpression of VEGF-C in LAPC-9 resulted in the development of lymph node and lung metastases. (*vi*) LAPC-4 and LAPC-9 tumor cells lacked expression of VEGFR-3 thus excluding the possibility of autocrine stimulation by VEGF-C of tumor cell invasiveness. Collectively, our findings indicate that VEGF-C-induced tumor lymphangiogenesis is sufficient to cause metastasis regionally (lymph nodes) and systemically (lungs) in low-metastatic prostate cancer models. Our data together with other studies suggest a central role for the lymphatic system in mediating prostate cancer metastasis.

Whether the prostate cancer metastasis is mediated by stimulation of intratumoral or peritumoral lymphangiogenesis or simply by activation of preexisting peritumoral lymphatics may however depend on the particular tumor aggressiveness and its microenvironment, as suggested by the differing observations obtained in experimental as well as in clinical studies.[18,38–41] For instance, a recent experimental study of the role of lymphangiogenesis and VEGF-C in prostate cancer metastasis suggested that peritumoral lymphatics, but not intratumoral lymphatics, contributed to lymph metastasis from an ortotopic site.[39] Theoretically, tumors developing *in situ* in the prostate may have immediate access to a more elaborate network of preexisting large lymphatics than tumors implanted in subcutaneous locations. Thus it is

possible that while the former may achieve access to the lymphatic network by expressing lymphangiogenic growth factors that act to enlarge and dilate preexisting lymph vessels,[42] the latter may depend more on genuine stimulation of lymphangiogenesis, either in the tumor periphery or intratumorally, to establish contact with the lymphatic network and generate lymphatic metastasis.

Evidently, other differences related to the tumor or its microenvironment may also contribute to the regulation of lymphatic metastasis. Particularly, stromal cell- (*e.g.*, fibroblasts, macrophages and immune cells) and extracellular matrix-derived factors in the tumor microenvironment may all contribute to tumor lymphangiogenesis, by producing pro-lymphangiogenic growth factors.[43] However, we found that the levels of tumor-associated macrophages were not significantly different between LAPC-9 control and LAPC-9/VEGF-C tumors (Fig. 4f), indicating that tumor VEGF-C production and lymphangiogenesis was mainly due to tumor cell-derived VEGF-C in this model.

Additionally, the precise requirement for the lymphatic system during dissemination of the tumor cells after they reach the local lymph nodes remains unclear, although several lines of evidence seem to suggest that lymphangiogenesis in the local lymph nodes may also play an important role during tumor metastasis.[44] Clearly, further studies are essential to determine the efficacy and timing of administering inhibitors of tumoral lymphangiogenesis in preventing prostate cancer metastasis, as well as to establish to what extent these treatments will be efficient to block intratumoral *versus* peritumoral lymphatic vessel-mediated tumor metastasis.

An essential component to evaluate antimetastatic therapies is to develop animal models, in which the process of tumor growth and metastasis can be effectively monitored. Whereas the ortotopic model has the great advantage of being a better model of the clinical situation, the subcutaneous implantation models allow for more straightforward surgical manipulation during tumor resection, as necessitated in our tumor models displaying a slow rate of metastasis. In this context it should be noted that surgical intervention carries a potential risk of iatrogenic tumor cell dissemination, although we consistently only have observed metastases in animals carrying LAPC-4 or LAPC9/VEGF-C tumors, and not in LAPC-9 controls, after tumor removal surgery. In our study we show that optical bioluminescence imaging as a tool to follow semiquantitatively the development over time of metastatic lesions in mice is both feasible and informative. Promisingly for the clinic, the high energy positron emission tomography (PET) modality has recently been applied successfully for noninvasive imaging of lymph node trafficking of lymphocytes,[45] and this technique may thus, in the future, be applied for *in vivo* detection of metastases in humans.

Taken together, these molecular imaging approaches should facilitate further prostate cancer studies to delineate the molecular steps involved in stimulation of lymphangiogenesis and lymphatic metastasis. An improved understanding of the complex regulation of these events may guide the development and evaluation of novel anti-lymphangiogenic agents in suppressing lymphatic and distant metastasis in prostate cancer patients.

Acknowledgments

This work is supported by NCI SPORE program P50 CA092131 (to Dr. L.W.) and the California Cancer Research Program 3NI0226 (to Dr. L.W.). Mr. J.B. is supported by UCLA RTPS Training program No. T32-GM008652 and Dr. E.B. by the Swedish Wenner-Gren Foundations. We appreciate Dr. John Colicelli (UCLA, Los Angeles, California) for providing materials for the generation of lentiviral constructs.

Grant sponsor: NCI SPORE program; Grant number: P50 CA092131; Grant sponsor: California Cancer Research Program; Grant number: 3NI0226; Grant sponsor: UCLA RTPS Training program; Grant number: No. T32-GM008652; Grant sponsor: Swedish Wenner-Gren Foundations.

References

1. National Cancer Institute. Cancer Stat Facts: Surveillance, Epidemiology, and End Results (SEER) Program. Rockville, MD: NCI; 2006.
2. D'Amico AV, Whittington R, Malkowicz SB, Fondurulia J, Chen MH, Kaplan I, Beard CJ, Tomaszewski JE, Renshaw AA, Wein A, Coleman CN. Pretreatment nomogram for prostate-specific antigen recurrence after radical prostatectomy or external-beam radiation therapy for clinically localized prostate cancer. J Clin Oncol 1999;17:168–72. [PubMed: 10458230]
3. Stone NN, Stock RG. Laparoscopic pelvic lymph node dissection in the staging of prostate cancer. Mt Sinai J Med 1999;66:26–30. [PubMed: 9989102]
4. Shah RB, Mehra R, Chinnaiyan AM, Shen R, Ghosh D, Zhou M, Macvicar GR, Varambally S, Harwood J, Bismar TA, Kim R, Rubin MA, et al. Androgen-independent prostate cancer is a heterogeneous group of diseases: lessons from a rapid autopsy program. Cancer Res 2004;64:9209–16. [PubMed: 15604294]
5. Pound CR, Partin AW, Eisenberger MA, Chan DW, Pearson JD, Walsh PC. Natural history of progression after PSA elevation following radical prostatectomy. JAMA 1999;281:1591–7. [PubMed: 10235151]
6. Roehl KA, Han M, Ramos CG, Antenor JA, Catalona WJ. Cancer progression and survival rates following anatomical radical retropubic prostatectomy in 3,478 consecutive patients: long-term results. J Urol 2004;172:910–14. [PubMed: 15310996]
7. Hull GW, Rabbani F, Abbas F, Wheeler TM, Kattan MW, Scardino PT. Cancer control with radical prostatectomy alone in 1,000 consecutive patients. J Urol 2002;167:528–34. [PubMed: 11792912]
8. Cheng L, Zincke H, Blute ML, Bergstralh EJ, Scherer B, Bostwick DG. Risk of prostate carcinoma death in patients with lymph node metastasis. Cancer 2001;91:66–73. [PubMed: 11148561]
9. Skobe M, Hawighorst T, Jackson DG, Prevo R, Janes L, Velasco P, Riccardi L, Alitalo K, Claffey K, Detmar M. Induction of tumor lymphangiogenesis by VEGF-C promotes breast cancer metastasis. Nat Med 2001;7:192–8. [PubMed: 11175850]
10. Stacker SA, Caesar C, Baldwin ME, Thornton GE, Williams RA, Prevo R, Jackson DG, Nishikawa S, Kubo H, Achen MG. VEGF-D promotes the metastatic spread of tumor cells via the lymphatics. Nat Med 2001;7:186–91. [PubMed: 11175849]
11. Achen MG, McColl BK, Stacker SA. Focus on lymphangiogenesis in tumor metastasis. Cancer Cell 2005;7:121–7. [PubMed: 15710325]
12. Mandriota SJ, Jussila L, Jeltsch M, Compagni A, Baetens D, Prevo R, Banerji S, Huarte J, Montesano R, Jackson DG, Orci L, Alitalo K, et al. Vascular endothelial growth factor-C-mediated lymphangiogenesis promotes tumour metastasis. Embo J 2001;20:672–82. [PubMed: 11179212]
13. Alitalo K, Carmeliet P. Molecular mechanisms of lymphangiogenesis in health and disease. Cancer Cell 2002;1:219–27. [PubMed: 12086857]
14. Zeng Y, Opeskin K, Baldwin ME, Horvath LG, Achen MG, Stacker SA, Sutherland RL, Williams ED. Expression of vascular endothelial growth factor receptor-3 by lymphatic endothelial cells is associated with lymph node metastasis in prostate cancer. Clin Cancer Res 2004;10:5137–44. [PubMed: 15297417]
15. Kaushal V, Mukunyadzi P, Dennis RA, Siegel ER, Johnson DE, Kohli M. Stage-specific characterization of the vascular endothelial growth factor axis in prostate cancer: expression of lymphangiogenic markers is associated with advanced-stage disease. Clin Cancer Res 2005;11:584–93. [PubMed: 15701844]
16. Zeng Y, Opeskin K, Horvath LG, Sutherland RL, Williams ED. Lymphatic vessel density and lymph node metastasis in prostate cancer. Prostate 2005;65:222–30. [PubMed: 15948136]
17. Tsurusaki T, Kanda S, Sakai H, Kanetake H, Saito Y, Alitalo K, Koji T. Vascular endothelial growth factor-C expression in human prostatic carcinoma and its relationship to lymph node metastasis. Br J Cancer 1999;80:309–13. [PubMed: 10390013]
18. Lin J, Lalani AS, Harding TC, Gonzalez M, Wu WW, Luan B, Tu GH, Koprivnikar K, VanRoey MJ, He Y, Alitalo K, Jooss K. Inhibition of lymphogenous metastasis using adeno-associated virus-mediated gene transfer of a soluble VEGFR-3 decoy receptor. Cancer Res 2005;65:6901–9. [PubMed: 16061674]

19. Jiang WG, Davies G, Martin TA, Parr C, Watkins G, Mansel RE, Mason MD. The potential lymphangiogenic effects of hepatocyte growth factor/scatter factor in vitro and in vivo. Int J Mol Med 2005;16:723–8. [PubMed: 16142411]
20. Craft N, Shostak Y, Carey M, Sawyers CL. A mechanism for hormone-independent prostate cancer through modulation of androgen receptor signaling by the HER-2/neu tyrosine kinase. Nat Med 1999;5:280–5. [PubMed: 10086382]
21. Craft N, Chhor C, Tran C, Belldegrun A, DeKernion J, Witte ON, Said J, Reiter RE, Sawyers CL. Evidence for clonal outgrowth of androgen-independent prostate cancer cells from androgen-dependent tumors through a two-step process. Cancer Res 1999;59:5030–6. [PubMed: 10519419]
22. Adams JY, Johnson M, Sato M, Berger F, Gambhir SS, Carey M, Iruela-Arispe ML, Wu L. Visualization of advanced human prostate cancer lesions in living mice by a targeted gene transfer vector and optical imaging. Nat Med 2002;8:891–7. [PubMed: 12134144]
23. Jenkins DE, Oei Y, Hornig YS, Yu SF, Dusich J, Purchio T, Contag PR. Bioluminescent imaging (BLI) to improve and refine traditional murine models of tumor growth and metastasis. Clin Exp Metastasis 2003;20:733–44. [PubMed: 14713107]
24. Klein KA, Reiter RE, Redula J, Moradi H, Zhu XL, Brothman AR, Lamb DJ, Marcelli M, Belldegrun A, Witte ON, Sawyers CL. Progression of metastatic human prostate cancer to androgen independence in immunodeficient SCID mice. Nat Med 1997;3:402–8. [PubMed: 9095173]
25. Morizono K, Xie Y, Ringpis GE, Johnson M, Nassanian H, Lee B, Wu L, Chen IS. Lentiviral vector retargeting to P-glycoprotein on metastatic melanoma through intravenous injection. Nat Med 2005;11:346–52. [PubMed: 15711560]
26. Dull T, Zufferey R, Kelly M, Mandel RJ, Nguyen M, Trono D, Naldini L. A third-generation lentivirus vector with a conditional packaging system. J Virol 1998;72:8463–71. [PubMed: 9765382]
27. Bhaumik S, Gambhir SS. Optical imaging of Renilla luciferase reporter gene expression in living mice. Proc Natl Acad Sci USA 2002;99:377–82. [PubMed: 11752410]
28. Brakenhielm E, Veitonmaki N, Cao R, Kihara S, Matsuzawa Y, Zhivotovsky B, Funahashi T, Cao Y. Adiponectin-induced antiangiogenesis and antitumor activity involve caspase-mediated endothelial cell apoptosis. Proc Natl Acad Sci USA 2004;101:2476–81. [PubMed: 14983034]
29. Cao R, Brakenhielm E, Pawliuk R, Wariaro D, Post MJ, Wahlberg E, Leboulch P, Cao Y. Angiogenic synergism, vascular stability and improvement of hind-limb ischemia by a combination of PDGF-BB and FGF-2. Nat Med 2003;9:604–13. [PubMed: 12669032]
30. Edinger M, Cao YA, Hornig YS, Jenkins DE, Verneris MR, Bachmann MH, Negrin RS, Contag CH. Advancing animal models of neoplasia through in vivo bioluminescence imaging. Eur J Cancer 2002;38:2128–36. [PubMed: 12387838]
31. Crowley CW, Cohen RL, Lucas BK, Liu G, Shuman MA, Levinson AD. Prevention of metastasis by inhibition of the urokinase receptor. Proc Natl Acad Sci USA 1993;90:5021–5. [PubMed: 8389464]
32. Cao Y, Linden P, Farnebo J, Cao R, Eriksson A, Kumar V, Qi JH, Claesson-Welsh L, Alitalo K. Vascular endothelial growth factor C induces angiogenesis in vivo. Proc Natl Acad Sci USA 1998;95:14389–94. [PubMed: 9826710]
33. Su JL, Yang PC, Shih JY, Yang CY, Wei LH, Hsieh CY, Chou CH, Jeng YM, Wang MY, Chang KJ, Hung MC, Kuo ML. The VEGF-C/ Flt-4 axis promotes invasion and metastasis of cancer cells. Cancer Cell 2006;9:209–23. [PubMed: 16530705]
34. De S, Chen J, Narizhneva NV, Heston W, Brainard J, Sage EH, Byzova TV. Molecular pathway for cancer metastasis to bone. J Biol Chem 2003;278:39044–50. [PubMed: 12885781]
35. Sramkoski RM, Pretlow TG II, Giaconia JM, Pretlow TP, Schwartz S, Sy MS, Marengo SR, Rhim JS, Zhang D, Jacobberger JW. A new human prostate carcinoma cell line, 22Rv1. In Vitro Cell Dev Biol Anim 1999;35:403–9. [PubMed: 10462204]
36. Holleran JL, Miller CJ, Culp LA. Tracking micrometastasis to multiple organs with lacZ-tagged CWR22R prostate carcinoma cells. J Histochem Cytochem 2000;48:643–51. [PubMed: 10769048]
37. Joukov V, Pajusola K, Kaipainen A, Chilov D, Lahtinen I, Kukk E, Saksela O, Kalkkinen N, Alitalo K. A novel vascular endothelial growth factor, VEGF-C, is a ligand for the Flt4 (VEGFR-3) and KDR (VEGFR-2) receptor tyrosine kinases. Embo J 1996;15:290–8. [PubMed: 8617204]

38. Roma AA, Magi-Galluzzi C, Kral MA, Jin TT, Klein EA, Zhou M. Peritumoral lymphatic invasion is associated with regional lymph node metastases in prostate adenocarcinoma. Mod Pathol 2006;19:392–8. [PubMed: 16400321]

39. Wong SY, Haack H, Crowley D, Barry M, Bronson RT, Hynes RO. Tumor-secreted vascular endothelial growth factor-C is necessary for prostate cancer lymphangiogenesis, but lymphangiogenesis is unnecessary for lymph node metastasis. Cancer Res 2005;65:9789–98. [PubMed: 16267000]

40. Trojan L, Rensch F, Voss M, Grobholz R, Weiss C, Jackson DG, Alken P, Michel MS. The role of the lymphatic system and its specific growth factor, vascular endothelial growth factor C, for lymphogenic metastasis in prostate cancer. BJU Int 2006;98:903–6. [PubMed: 16978291]

41. Hoshida T, Isaka N, Hagendoorn J, di Tomaso E, Chen YL, Pytowski B, Fukumura D, Padera TP, Jain RK. Imaging steps of lymphatic metastasis reveals that vascular endothelial growth factor-C increases metastasis by increasing delivery of cancer cells to lymph nodes: therapeutic implications. Cancer Res 2006;66:8065–75. [PubMed: 16912183]

42. Zeng Y, Opeskin K, Goad J, Williams ED. Tumor-induced activation of lymphatic endothelial cells via vascular endothelial growth factor receptor-2 is critical for prostate cancer lymphatic metastasis. Cancer Res 2006;66:9566–75. [PubMed: 17018613]

43. Schoppmann SF, Birner P, Stockl J, Kalt R, Ullrich R, Caucig C, Kriehuber E, Nagy K, Alitalo K, Kerjaschki D. Tumor-associated macrophages express lymphatic endothelial growth factors and are related to peritumoral lymphangiogenesis. Am J Pathol 2002;161:947–56. [PubMed: 12213723]

44. Hirakawa S, Kodama S, Kunstfeld R, Kajiya K, Brown LF, Detmar M. VEGF-A induces tumor and sentinel lymph node lymphangiogenesis and promotes lymphatic metastasis. J Exp Med 2005;201:1089–99. [PubMed: 15809353]

45. Shu CJ, Guo S, Kim YJ, Shelly SM, Nijagal A, Ray P, Gambhir SS, Radu CG, Witte ON. Visualization of a primary antitumor immune response by positron emission tomography. Proc Natl Acad Sci USA 2005;102:17412–7. [PubMed: 16293690]

Abbreviations

FL	firefly luciferase
LYVE-1	lymph vessel endothelial hyaluronan receptor-1
MOI	multiplicity of infection
PSA	prostate specific antigen
ROI	region of interest
RL	renilla luciferase
SCID	severe combined immune-deficient
VEGF-A	vascular endothelial growth factor-A
VEGF-C	vascular endothelial growth factor-C
VEGFR-3	vascular endothelial growth factor receptor-3

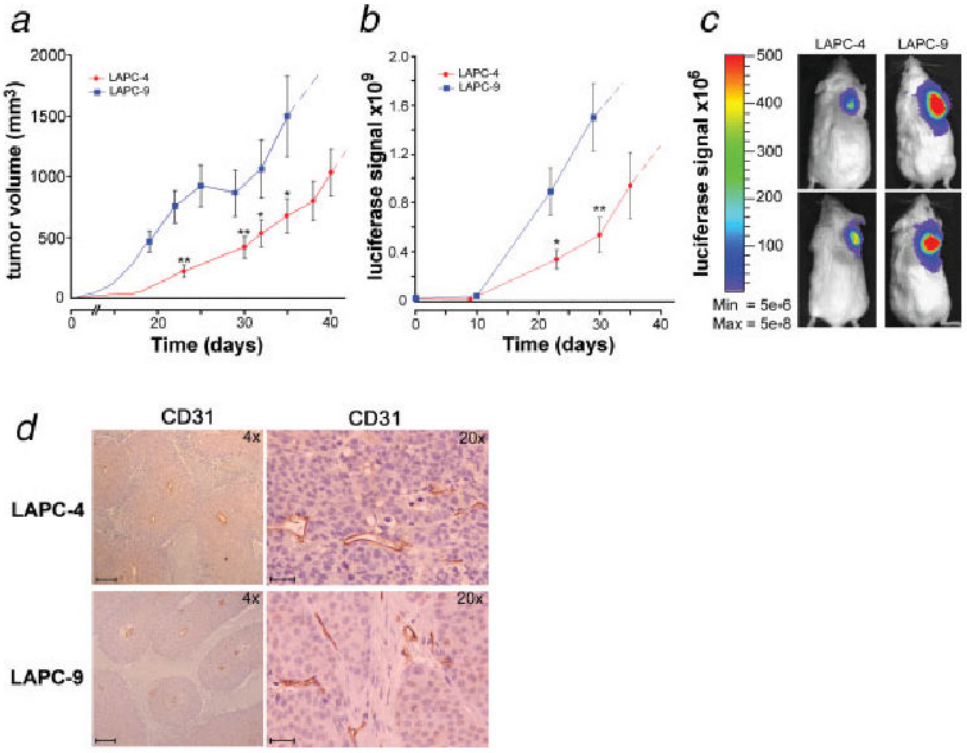

Figure 1.

Prostate cancer xenograft models: optical imaging of tumor growth. LAPC-4 and LAPC-9 human tumor cells were implanted in immune-deficient mice (n = 10). Tumor volume was measured (*a*) and the luciferase reporter gene (FL) activity assayed *via in vivo* optical imaging (*b*). Blue color = LAPC-9 group; red color = LAPC-4 group. Dashed extensions of the curves represent projected values after tumors had been surgically removed in the majority of animals in a group. Representative examples of the tumor-derived optical signal in LAPC-4- and LAPC-9-bearing mice at day 20 postimplantation are shown (*c*). The color bar indicates the intensity range of the bioluminescence signal (p/s/cm^2/sr). The tumors were surgically removed within 4–7 weeks postimplantation. Immunohistochemical staining of blood vessels in tumor sections revealed no difference in vascularity between the groups (*d*; ×4 and ×20). Scale bars = 200 and 50 μm, respectively.

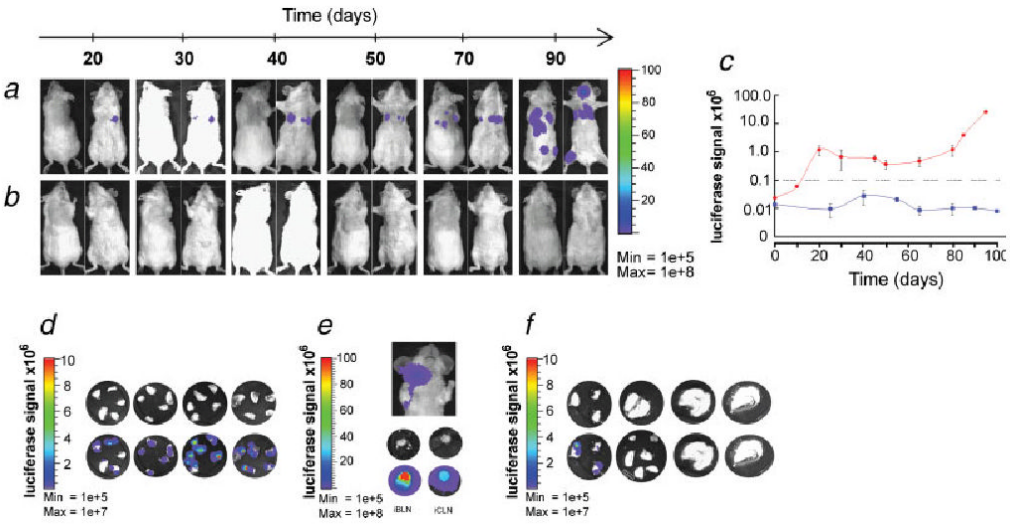

Figure 2.

Tumor metastasis monitored by *in vivo* and *ex vivo* optical imaging. Representative examples of dorsal and ventral optical images of mice in the LAPC-4- (*a*) and LAPC-9 cohort (*b*) at various time points following primary tumor resection are shown. The appearance of bioluminescence signal above background was first evident in the ventral side of the mice, suggestive of lung metastases. The color bar to the right indicates the signal intensity range (p/s/cm^2/sr × 10^6). The maximal luciferase signal emitted from the ventral side of animals in LAPC-4- and LAPC-9 groups is plotted over time after tumor removal (*c*). The grey dashed line shows the level set for background signal. Only LAPC-4-implanted mice developed *in vivo* signals indicative of metastasis. These secondary sources of bioluminescence emission in the animals remained stable or increased in intensity over time. Blue color = LAPC-9 group; red color = LAPC-4 group. Data represent averages ±SEM (*n* = 4). Within 100 days after the tumor removal the animals were sacrificed and the lungs and lymph nodes dissected and imaged optically for the presence of tumor cell-derived luciferase signal. Lung metastatic signs were observed in all but one of the LAPC-4- (*n* = 9) and in only one of the LAPC-9-implanted mice (*n* = 7), whereas lymph node signals were found in three LAPC-4 mice and in one LAPC-9 mouse (see Table I). Representative examples of lungs (*d*) and lymph nodes (*e*) from the LAPC-4 group and lungs (*f*) from the LAPC-9 group are shown. The color scale indicates bioluminescence intensity (p/s/cm^2/sr). The upper row circular microphotographs are each from a different animal, and the lower row pictures are the corresponding bioluminescence composite images. iBLN, ipsilateral brachial lymph node; iCLN, ipsilateral cervical lymph node.

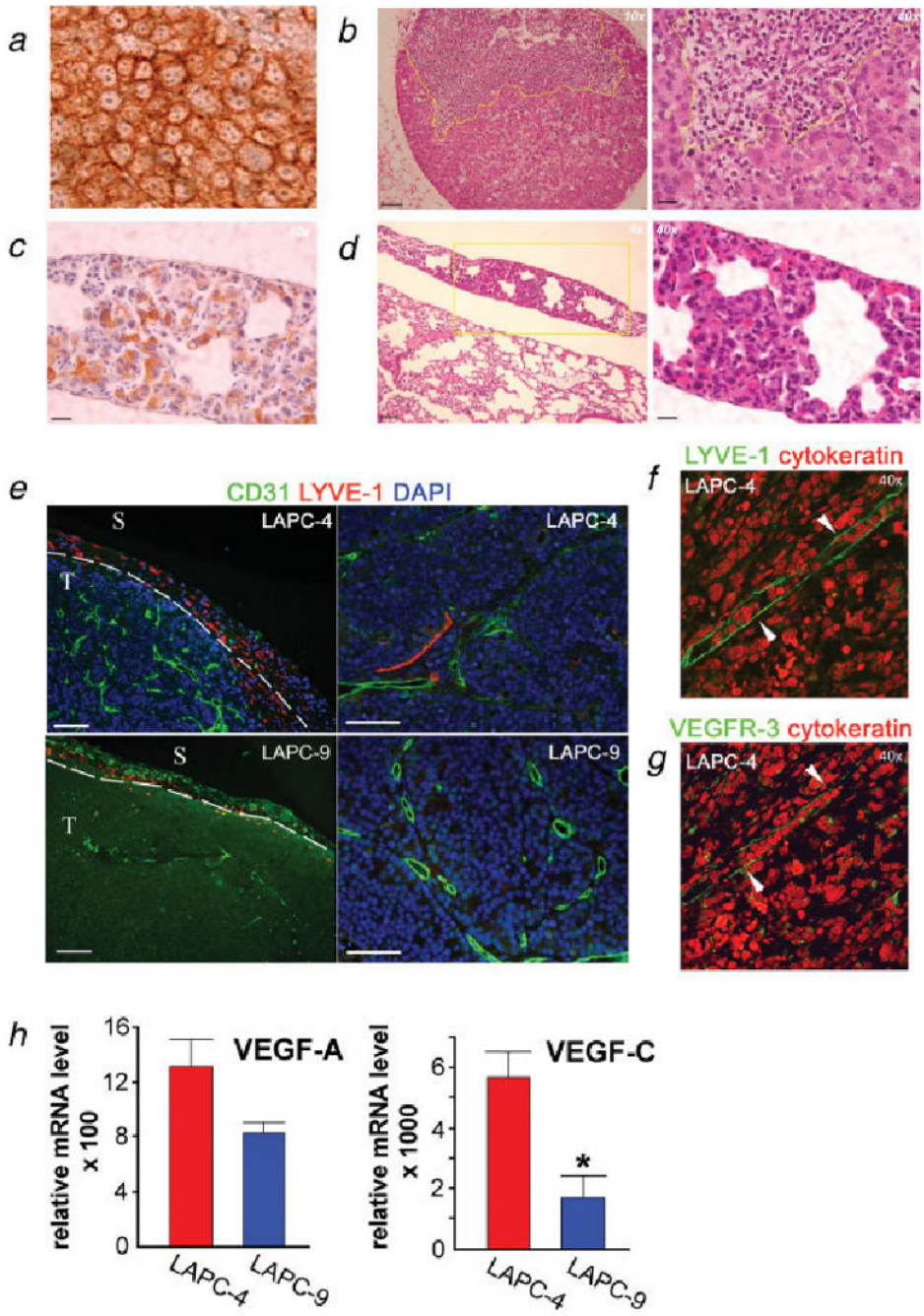

Figure 3.

Immunohistochemical detection of metastases and studies of angiogenic and lymphangiogenic tumor profiles. Lung and lymph node sections from LAPC-4- and LAPC-9-implanted mice were processed to detect tumor cells in the parenchyma. LAPC-4 primary tumor sections served as positive controls for human cytokeratin (*a*). Hematoxylin & eosin stained sections revealed tumor metastases in the lymph nodes (*b*) and lungs (*d*) from the LAPC-4 group. A brachial lymph node from a LAPC-4-implanted mouse shows a large subcapsular lesion (*b*). Cytokeratin staining revealed tumor cells present in lungs in the LAPC-4-implanted group (*c*). Yellow lines indicate the tumor mass. Scale bars = 200 μm (×4), 100 μm (×10) and 25 μm (×40), respectively. The blood (CD31; green) and lymph (LYVE-1; red) vessels of the

primary tumors (nuclei, blue) were visualized by immunohistochemistry. Analysis of LAPC-4 tumors revealed the presence of small lymphatics both in peritumoral and intratumoral areas (*e*, left: ×10 and right: ×20; *f*, ×40). Most LAPC-9 tumors displayed only very few lymphatic vessels at the tumor periphery (*e*, left: ×10). Scale bar in *e* = 100 μm. T, tumor; S, surrounding tissue. The intratumoral LYVE-1 positive (green) structures (f, ×40, white arrowheads) were also positive for another lymphatic marker, VEGFR-3 (green) (*g*, ×40, white arrowheads). Angiogenic and lymphangiogenic growth factor expressions were analyzed in the excised tumors by real time RT-PCR analysis (*h*). VEGF-A levels were found to be similar whereas VEGF-C expression levels were significantly and markedly elevated in LAPC-4 as compared to LAPC-9 tumors. $*p < 0.05$.

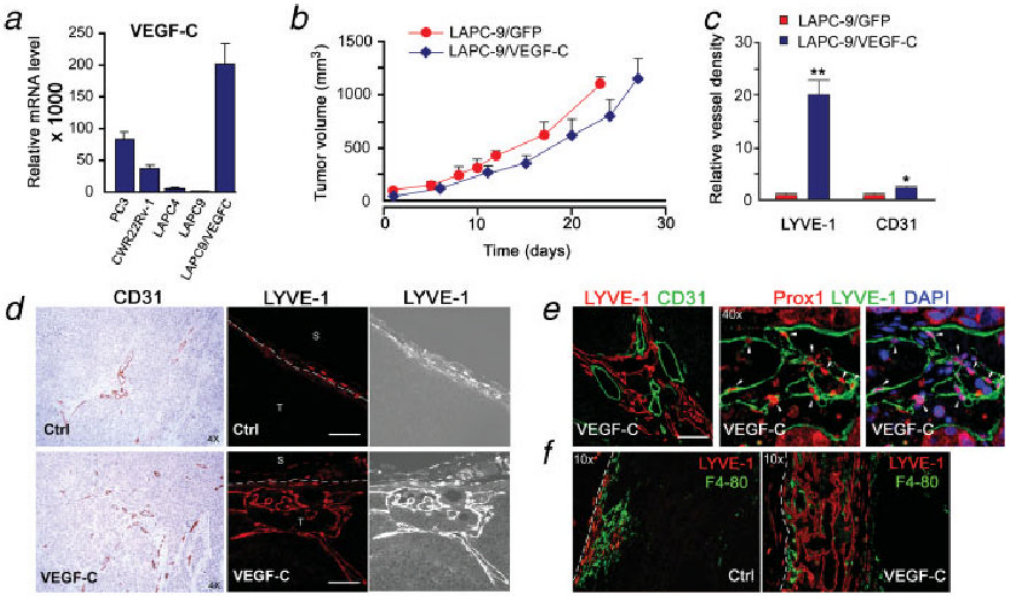

Figure 4.

VEGF-C expression enhances intratumoral lymphangiogenesis in LAPC-9. VEGF-C expression was determined by real time RT-PCR analysis of various prostate cancer tumor samples (*a*). Overexpression of VEGF-C in LAPC-9 results in > 100-fold increase in VEGF-C levels as compared to LAPC-9/GFP tumors. This is ~ 2-fold and 4-fold higher levels as compared to PC3 and CWR22Rv-1, respectively. Primary tumor growth rates in immune-deficient mice were similar in LAPC-9/GFP- and LAPC-9/VEGF-C-implanted mice (*b; n* = 6–8). Tumor immunohistochemical examination revealed that blood vessels (CD31; ×4) and in particular intratumoral lymphatic vessels (LYVE-1, ×20) were more abundant in LAPC-9/VEGF-C tumors as compared to LAPC-9/GFP control tumors (*c*, *d*; S, surrounding tissue; T, tumor). Quantification analysis demonstrated that the lymphatic vessel density in LAPC-9/VEGF-C tumors (VEGF-C, blue) was 20-fold higher than in LAPC-9/GFP control tumors (Ctrl, red) (*c*; LYVE-1), whereas there was only a modest 2-fold increase in blood vessel density (*c*; CD31). Double staining for lymph (LYVE-1, red) and blood vessels (CD31, green) in LAPC-9/VEGF-C tumors revealed extensive networks of intratumoral lymph vessels growing in proximity to blood vessels (*e*, left: ×20). LYVE-1 positive structures (green) were also positive for another lymphatic marker, prox1 (red) (*e*, center and right, ×40, white arrowheads). LYVE-1 positive cells (red) did not colocalize with a macrophage marker F4/80 (green) (*f*, ×10). White scale bars in *d*, *e* = 100 μm; **p* < 0.05, ***p* < 0.005.

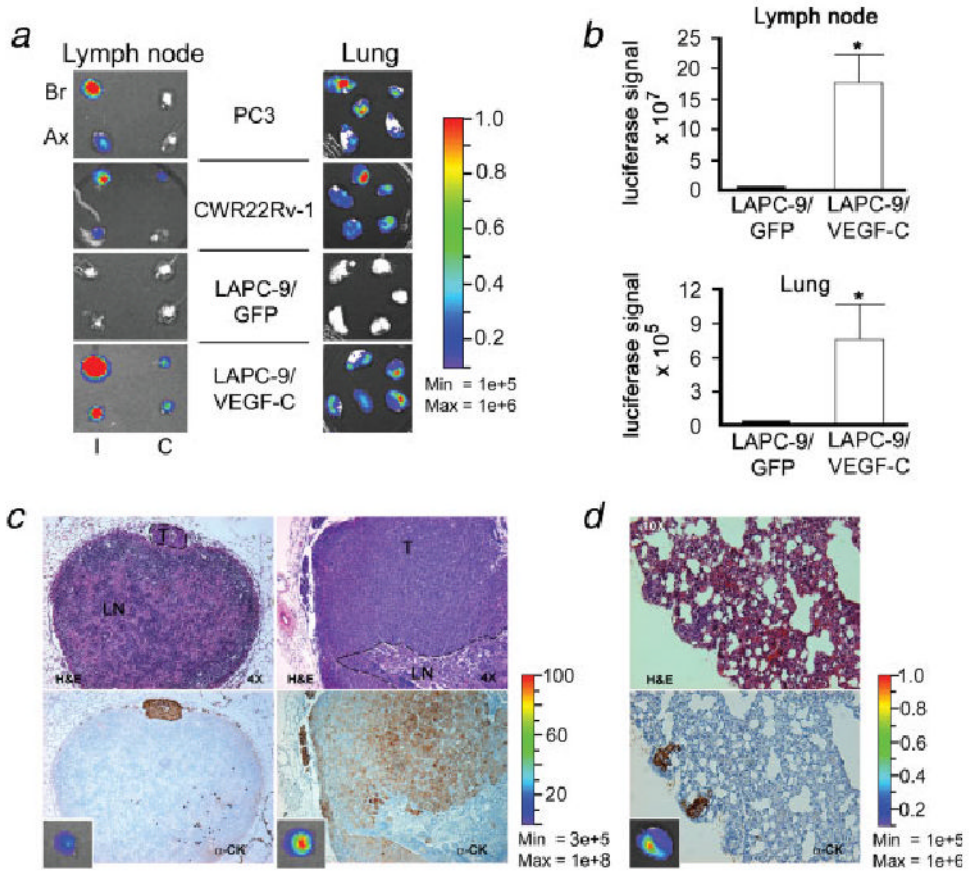

Figure 5.

VEGF-C expression levels correlate with development of lymph node and lung metastases. Different human prostate cancer cells were implanted in immune-deficient mice (n = 6–8). At sacrifice, the luciferase reporter gene (RL) activity was assayed *ex vivo* by optical imaging of dissected organs. Representative examples of bioluminescence images of lymph nodes and lungs are shown (*a*, I, ipsilateral, C, contralateral, Br, brachial lymph node, Ax, axillary lymph node). The color bars indicate the intensity range of the bioluminescence signal (p/s/cm^2/sr × 10^6). The mice bearing PC3 and CWR22Rv-1 tumors showed extensive metastasis to regional lymph nodes and lungs, whereas LAPC-9/GFP control tumors did not metastasize. Overexpression of VEGF-C in LAPC-9 resulted in intense luciferase signals in both lymph nodes and lungs, suggestive of metastasis. Quantification analysis of bioluminescence revealed that the optical signals were ~ 100-fold higher in regional lymph nodes and ~ 20-fold higher in lungs from LAPC-9/VEGF-C-implanted mice as compared to LAPC-9-implanted control mice (*b*). Hematoxylin & eosin (H&E, upper panel) and cytokeratin (α-CK, lower panel) staining of tissue sections confirmed the presence of tumor metastases in the lymph nodes (*c*; T, tumor; LN, lymph node, ×4) and lungs (*d*; ×10) from the LAPC-9/VEGF-C-implanted group. The corresponding whole organ optical imaging photo for each sample is shown in the small insert in the lower panels (*c*, *d*). The color bars indicate the intensity range of the bioluminescence signal (p/s/cm^2/sr × 10^6). *p < 0.05.

Table I

Number Of Mice With Luciferase Positive Lungs Or Lymph Nodes (Ln) At Sacrifice As Judged By *Ex Vivo* Optical Imaging

Degree of involvement	LAPC-4	LAPC-9
Lungs		
No metastasis	1	6
1–2 Positive lobes	2	0
3–4 Positive lobes	1	1
All lung lobes positive	5	0
Incidence of lung metastasis	**89%**	**14%**
Lymph nodes		
No metastasis	6	6
Positive brachial LNs	2	1
Positive cervical LNs	3	0
Incidence of LN metastasis	**33%**	**14%**

In the LAPC-4 implanted mice 2 out of 9 mice had both brachial and cervical lymph node metastases. The total number of animals with luciferase positive lymph nodes in the LAPC-4 group was 3 animals.